特约专栏

Influence of Initial Surface Area/Volume Ratio of the Fiber Preform on Kinetics of Chemical Vapor Infiltration and Texture of Infiltrated Carbon

ZHANG Weigang[1,2], Huettinger K J[1]

(1. Institute of Chemical Technology and Polymer Chemistry, Karlsruhe Institute of Technology, Karlsruhe 76131, Germany)

(2. State Key Laboratory of Multiphase Complex Systems, Institute of Process Engineering, CAS, Beijing 100190, China)

Abstract: Isothermal, isobaric chemical vapor infiltration of carbon fiber felts with fiber volume fractions of 7.1% and 14.2% were investigated to analyze the influence of initial surface area / volume ratio, [A/V], of the fiber preform on infiltration kinetics and texture of infiltrated carbon. Experiments were performed at a temperature of 1 095 ℃, a methane pressure of 22.5 kPa, a residence time of 0.1 s and infiltration times being stepwise increased from 20 to 120 h. Global bulk density and bulk density, porosity as well as density of matrix carbon as a function of infiltration depth were determined. Carbon texture was analyzed with polarized-light microscopy. The results show that infiltration kinetics in the initial stage of infiltration are dominated by the nucleation mechanism and afterwards by the growth mechanism of carbon formation. These changes of deposition chemistry and kinetics lead to changes of carbon texture from low / medium to medium / high. All changes are caused by an increase of [A/V] ratio. They occur in a significantly earlier stage in the case of the felt with the higher initial [A/V] ratio, as to be expected. These results are a perfect confirmation of conclusions from earlier studies.

Key words: pyrolytic carbon; chemical vapor infiltration; mercury porosimetry; optical microscopy; texture

CLC number: TB323 Document code: A Article ID: 1674 - 3962(2013)11 - 0646 - 09

碳纤维预制体的初始 A/V 值对化学气相渗透动力学和热解碳结构的影响

张伟刚[1,2], Huettinger K J[1]

(1. 卡尔斯鲁厄理工学院 化学技术与高分子化学研究所, 德国 卡尔斯鲁厄 76131)

(2. 中国科学院过程工程研究所 多相复杂系统国家重点实验室, 北京 100190)

摘 要: 采用体积含量分别为 7.1% 和 14.2% 的两种碳纤维各向同性针刺毡为预制体, 研究了预制体内部初始碳纤维表面积与自由体积比值(A/V 值)对热解碳的等温等压化学气相渗透动力学以及热解碳织态结构变化的影响。实验研究以 22.5 kPa 纯甲烷为碳源气体, 沉积温度为 1 095 ℃, 气体平均停留时间 0.1 s, 沉积时间从 20 h 到 120 h 不等。热解碳沉积后测量了 C/C 复合材料的表观密度、开气孔率、热解碳的真密度及其内部分布。利用正交偏光显微镜测试了热解碳的织态结构。研究结果表明, 热解碳的初始沉积过程主要受气相 - 表面形核机制控制, 随着致密化的进行, 逐渐转变为表面生长机制。这种从形核到表面生长机制的转化, 导致了热解碳的织态结构相应地从低织构向中织构、最后到高织构的转化。上述沉积机制和结构的变化, 都是由于碳纤维编制体初始 A/V 值的不同以及由于热解碳不断沉积导致的 A/V 值的不断增大引起的。增大碳纤维编制体的初始 A/V 值, 可以导致这些转化在致密化过程中提前发生。上述结果能够很好地证明以前相关研究的结论。

关键词: 热解碳; 化学气相渗透; 压汞仪孔隙率测试; 光学显微镜; 织态结构

1 Introduction

Significant progress has been made in understanding kinetics and texture formation in chemical vapor deposition

收稿日期: 2013 - 07 - 01

第一作者及通信作者: 张伟刚, 男, 1968 年生, 研究员

DOI: 10.7502/j.issn.1674 - 3962.2013.11.02

(CVD) of carbon from methane being the privileged carbon precursor for chemical vapor infiltration (CVI)[1-22]. Both, kinetics and texture of carbon are controlled not only by the classical parameters of temperature, pressure or partial pressure and residence time, because carbon is formed from the precursor gas not in a direct reaction, but in complex consecutive and parallel reactions occurring as homogeneous reactions in the gas phase as well as heterogeneous reactions at the surface of the substrate[1-2]. As (Eq. 1):

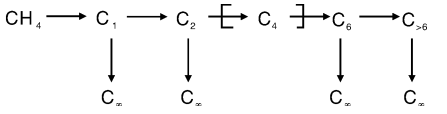

(1)

With $C_1 = CH_3$; $C_2 = C_2H_6 \cdots\cdots C_2H_2$; $C_4 = C_4H_6 \cdots\cdots C_4H_4$; C_6 = monocyclic aromatic hydrocarbons; $C_{>6}$ = polycyclic aromatic hydrocarbons; C_∞ = carbon

With this knowledge it was necessary to introduce the surface area / volume ratio, [A/V], of the deposition space as an additional parameter describing the interaction or competition between homogeneous and heterogeneous reactions[1]. In fact, the [A/V] ratio corresponds to a volume related concentration of active sites the latter value resulting from the product of volume related surface area and surface related concentration of active sites. At a low or very low [A/V] ratio surface reactions are unimportant and the overall reaction is dominated by gas phase reactions leading to aromatic hydrocarbons and finally to soot. Surface or heterogeneous reactions are prevailing at high ratios favoring reactions of reactive species from the gas phase with active sites at the substrate surface, which simultaneously limits the formation of larger species in the gas phase. This case is typical for the CVI of carbon fiber preforms.

The influence of [A/V] ratio on the deposition chemistry has direct consequences on the kinetics of deposition as well as the texture of carbon. High ratios lead to low surface related deposition rates because carbon is preferentially formed from small species. Decreasing ratios cause a shift of deposition chemistry from small, mainly C2-species, to larger, aromatic hydrocarbon species and thus to increasing surface related deposition rates[23].

A change of deposition chemistry by varying [A/V] ratios also effects changes of texture formation of carbon. According to the particle-filler model, derived for the so-called growth mechanism of carbon formation[24, 18], high-textured carbon is only formed at a special ratio of small linear, mainly C2-species and small aromatic hydrocarbon species, preferentially one-and two-membered ring species. This implies that less textured, medium-to low-textured carbon has to be expected at increasing as well as decreasing ratios corresponding to increasing or decreasing [A/V] ratios.

These conclusions have already been confirmed in experimental studies and numerical simulations of the CVI process[14-16, 18-19]. CVI studies of a carbon fiber felt with a fiber volume fraction of 7.1% at 1 095 ℃ and various methane pressures showed a high-textured matrix carbon at a pressure of about 10 kPa[18]; corresponding studies with a 2D carbon fiber preform with a fiber volume fraction of 22.5% yield a similar or equal high-textured carbon at a higher methane pressure of about 22.5 kPa[19]. An inside-outside densification was observed with both preforms. The results demonstrate that a higher initial [A/V] ratio of the 2D carbon fiber preform can be compensated using a higher methane pressure which obviously produces the optimum ratio between C2-and small aromatic hydrocarbon species.

Inside-outside densification was also confirmed in model studies with capillaries 1 mm in diameter and 16 and 32 mm in depth. Ratios of deposition rates in the depth and at the mouth of the capillaries up to 10 (16 mm) and 20 (32 mm) were determined[15]. Numerical simulations of CVI of capillaries considering the complex gas phase chemistry with simplified chemical models showed that the above ratio of deposition rate is increasing with increasing depth and the diameter of the capillary, increasing complexity of consecutive reactions in the gas phase, and increasing methane pressure[14,16]. The beneficial effect of increasing capillary depth and increasing pressure is limited up to optimum values. Texture analyses of the deposited carbon in the above experimental studies with capillaries revealed formation of high-textured carbon at low methane pressures in the range from 5 to 6 kPa. This result on texture is in perfect agreement with the results obtained with the felt and 2D preform, because the initial [A/V] ratio of the capillary of 4 mm^{-1} is much smaller.

The present study is concerned with CVI of carbon fiber preforms based on the same fiber architecture, a felt with nearly random orientation of the fibers, but exhibiting different fiber volume fractions of 7.1 and 14.2%, and correspondingly different [A/V] ratios of 33 and 71 mm^{-1}. These preforms were infiltrated at identical conditions, a temperature of 1 095 ℃, a methane pressure of 22.5 kPa and a residence time of 0.1 s. Infiltration times were stepwise increased from 20 to 120 h, not studied in the earlier investigations with various pressures. For analysis of kinetics, bulk density and pore size distribution were determined in all steps of infiltration. The texture of the infiltrated carbon was characterized by determination of the matrix density and the extinction angle, A_e, using polarized-light microscopy (PLM).

2 Experimental

2.1 infiltration conditions

Reactor and sample holder used in the study are the same as used in earlier CVI studies[18-19]. The rectangularly shaped felt sample, 42 mm in length, 16 mm in width and 40 mm in height, is fitted in a cylindrically shaped sample holder, 45 mm in diameter and made from high-purity graphite. With the aid of the sample holder the gas flow is limited to a narrow annulus, about 2 mm in width. According to the length of the felt of 42 mm the infiltration depth amounts to 21 mm because infiltration is carried out from both sides, as shown in Fig. 1. The gas flows from the bottom to the top. The residence time of the gas, corresponding to the height of the felt of 40 mm, amounts to 0.1 s without considering a volume increase caused by partial decomposition of methane. Infiltration conditions are 1 095 ℃ and 22.5 kPa.

The felt used is identical to that used in the earlier study[18]. The fiber is based on viscose and exhibits a density of 1.72 g/cm^3. The as-procured felt exhibits a fiber volume fraction of 7.1% (≡ Felt I). A fiber volume fraction of 14.2% (≡ Felt II) was achieved by compressing the original Felt I.

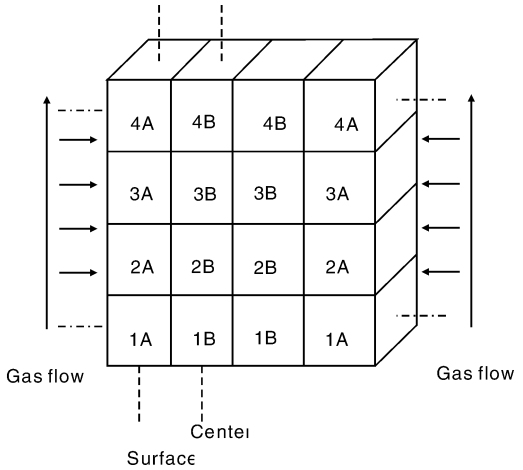

Fig. 1 Scheme showing the infiltration and preparation of samples from an infiltrated bloc

2.2 Preparation of samples and analytical methods

After each infiltration run the average bulk density was determined from mass and volume. The bloc was then cut into 16 samples, as shown in Fig. 1, to determine bulk density and pore size distribution of the individual samples. For mercury porosimetry studies a set of two samples had to be used, samples 2A and 3A for the outer region ("surface") and samples 2B and 3B for the inner region ("center"). Mercury porosimetry yields some further parameters such as bulk density, skeletal density, cumulative pore volume and surface area. With these data the density of the infiltrated carbon including closed porosity ("matrix density") can be determined with Eq. (2):

$$\rho_{matrix} = \frac{\rho_{bulk} - \delta_F \cdot \rho_{Fiber}}{\rho_{bulk} - \delta_F \cdot \rho_{skeleton}} \cdot \rho_{skeleton} \qquad (2)$$

ρ_{matrix}, ρ_{bulk} and $\rho_{skeleton}$ are matrix, bulk and skeletal density, respectively. ρ_{Fiber} and δ_F are the density of carbon fiber and its volume fraction, 1.72 g/cm^3, 7.1% and 14.2%, respectively.

The texture of infiltrated carbon was studied with polarized-light microscopy (PLM) at cross-sections 1A and 4B as shown in Fig. 1. For a quantitative description of carbon texture the extinction angle, A_e, was determined[25-29]. In the case of a completely circular fiber cross-section the error is about ±1°. Because the fibers in the felt are not really circular (see later) the error is in the range of about ±1.5°.

3 Results

3.1 Densification

Average bulk densities of Felt I and II as a function of infiltration time are shown in Fig. 2. A fast densification of the felts occurs within the first 60 h leading to a bulk density of about 1.6 g/cm$_3$. Maximum densities of 1.818 g/cm$_3$ are obtained after 120 h. This maximum density is lower than 1.92 g/cm$_3$ obtained with Felt I using the same temperature and residence time, but a methane pressure of 10 kPa[18]. Reasons will be discussed later.

Increasing bulk density corresponds to an increasing mass. This means that the deposition rate of carbon is constant up to about 40 h and, even more remarkable, nearly the same for both felts. This underlines that the deposition rate is not controlled by the surface area.

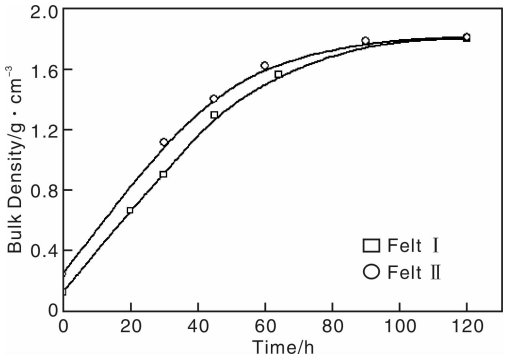

Fig. 2 Bulk densities of Felt I with a fiber volume fraction of 7.1% and Felt II with a fiber volume fraction of 14.2% as a function of infiltration time

Bulk densities as a function of infiltration depth were determined in various heights of the infiltrated felts (layer 1 to 4; see Fig. 1) after infiltration times of 30, 64 (Felt I) (60, Felt II) and 90 h. The results are presented in Fig. 3a, b, c (Felt I) and Fig. 4a, b, c (Felt II). Higher densities in the

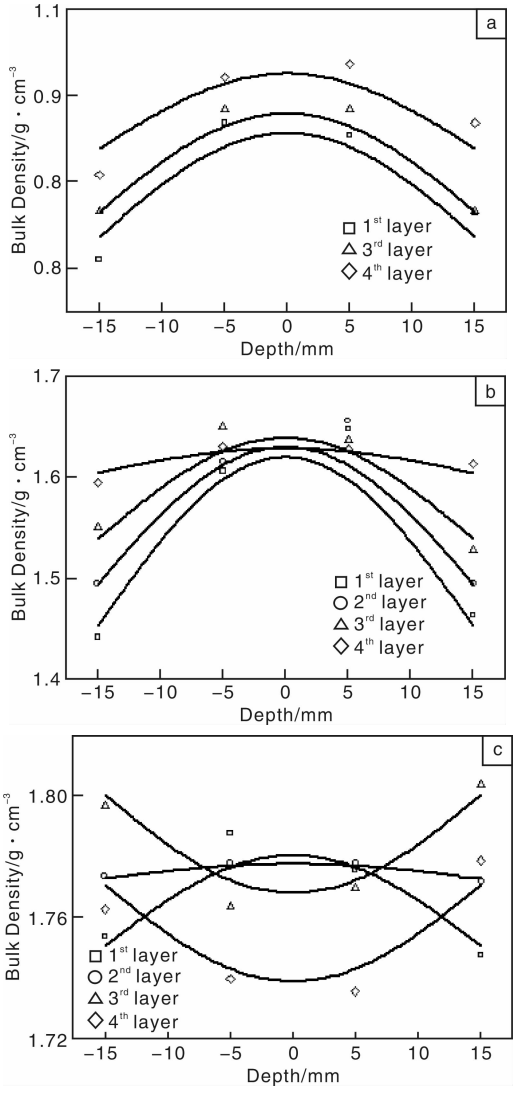

Fig. 3 Profiles of bulk density at various infiltration times and heights versus depth of Felt I: (a) 30 h, (b) 64 h, and (c) 90h

center (maximum infiltration depth) are a consequence of higher deposition rates and thus an inside-outside densification as already reported in earlier studies[18-19]. This type of densification occurs up to 64 (60) h in all heights of both felts (Fig. 3a, b and Fig. 4a, b). After 90 h this can only be observed in the case of Felt II (Fig. 4c) indicating a significant influence of the initial [A/V] ratio on the densification behavior.

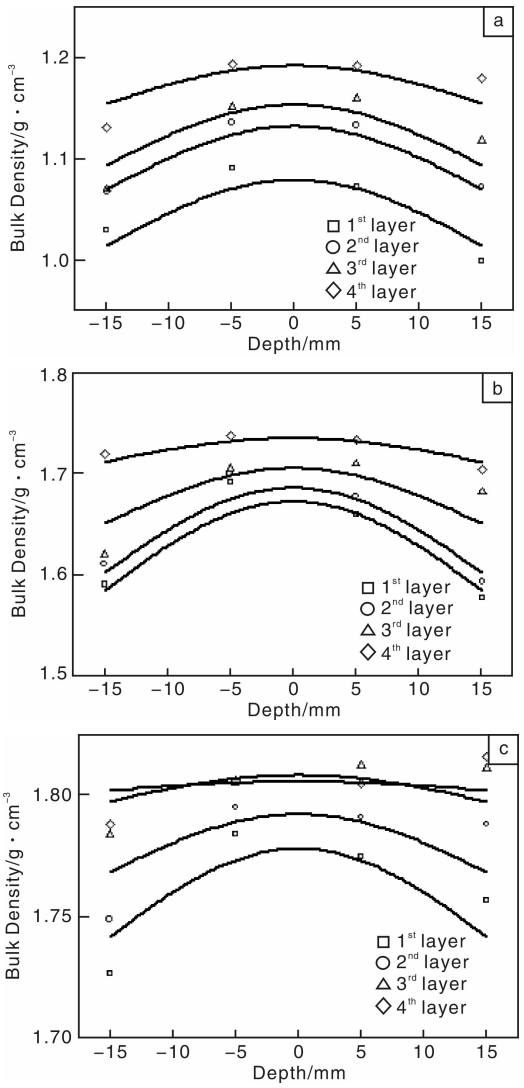

Fig. 4 Profiles of bulk density at various infiltration times and heights versus depth of Felt II: (a) 30 h, (c) 64 h, and (c) 90 h

Densities at the surface (±15 mm) increase with increasing height of the felt which can clearly be attributed to higher relative residence times and thus progressive decomposition reactions of methane flowing from the bottom to top of the reactor. These decomposition reactions outside the felt are also responsible for decreasing density gradients between center and surface from the lower to the upper part of the felt (layer 1 to 4). The gradients reflect the ratio of methane decomposition outside and inside of the felt caused by different residence time ratios. It is evident that this ratio is the highest in the first layer and the lowest in the fourth layer. These results demonstrate that high or very high flow rates of methane are a decisive criterion for an inside-outside densification of the fiber preform.

Mercury porosimetry studies were mainly performed to calculate the density of the deposited carbon (Eq. (2)), because density is an important measure for the crystallinity or texture of carbon. Pore size distributions resulting from the studies are presented in Fig. 5a and 5b. It shows the average cumulative pore volume in the "center" and at the "surface" of layers 2 and 3 (see Fig. 1) as a function of pore entrance diameter down to 0.1 μm after infiltration times of 45, 64 (60) and 90 h. Results for the "center" and "surface" were produced using combined samples 2B and 3B or 2A and 3A, respectively. Pores smaller than 0.1 μm are not considered because an infiltration at longer times seems to be relatively improbable.

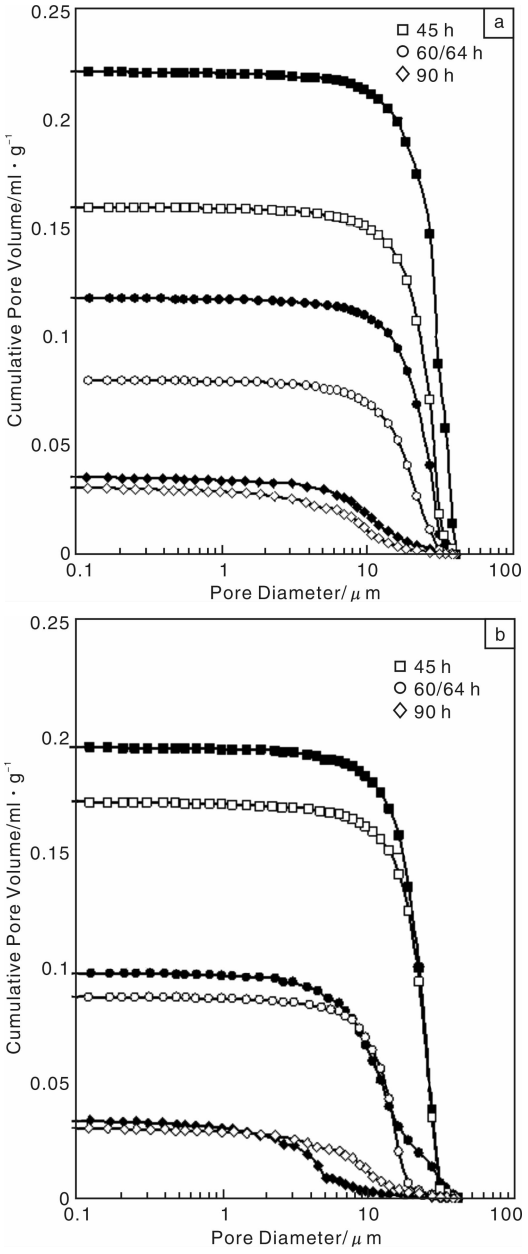

Fig. 5 Cumulative pore volume of Felt I (a) and Felt II (b) after various infiltration times. open symbols: center region and closed symbols: surface region

Results with both felts show that porosity is mainly formed from pores with entrance diameters from about 40 μm to about 5 μm. Additional porosity with smaller pores is only generated in the final stage of infiltration (90 h). Pore volumes are generally higher at the "surface", the difference in pore volume between "surface" and "center" being decreasing with progressive infiltration. This tendency is in agreement with the differences in bulk densities. It is also remarkable that Felt II shows significant smaller differences compared to Felt I.

The density of deposited carbon (matrix density) was estimated using Eq. (2) and necessary data from mercury porosimetry. Resulting density values represent a lower limit because closed pores and open pores smaller than 3 nm (limits of mercury porosimetry at a maximum pressure of 200 MPa) can not be considered. Results based on Samples 2B and 3B ("center") and 2A and 3A ("surface") are presented in Fig. 6a and 6b. It shows the corresponding average matrix densities as a function of infiltration time up to 120 h. It is obvious that densities obtained in the infiltration of Felt II are significantly higher than those of Felt I, and additionally nearly independent of infiltration time. This result indicates a deposition of carbon with the same, more or less high texture degree from the beginning of infiltration up to complete densification. Densities in the center are slightly higher.

Completely different results were obtained with Felt I. Carbon with relatively low density is deposited in the initial stages of infiltration followed by a substantial density increase. It is even more interesting that carbon deposited at the "surface" exhibits a higher density than carbon deposited in the "center".

An interpretation of these results with Felt I and II is only possible with the aid of texture analyses presented in the following. Nevertheless, it can be concluded that the [A/V] ratio has an even more tremendous effect on the kind of deposited carbon than on kinetics of densification.

3.2 Texture of infiltrated carbon

The texture of matrix carbon was investigated in cross-sections of sample 1A to 4A ("surface": bottom to top) and sample 1B to 4B ("center": bottom to top) using polarized-light microscopy. The micrographs shown in Fig. 7 (Felt I) and Fig. 8 (Felt II) correspond to cross-sections in 1A and 4B which usually show the most pronounced differences of the matrix carbon. Samples after infiltration times of 30, 45, 64 (60), 90 and 120 h (Felt II) were investigated.

Two carbon layers are generally formed around the fibers in both felts, a low-to medium-textured first layer and a medium-to high-textured second layer. Texture changes are occurring relatively abruptly as already known from earlier studies[30-33].

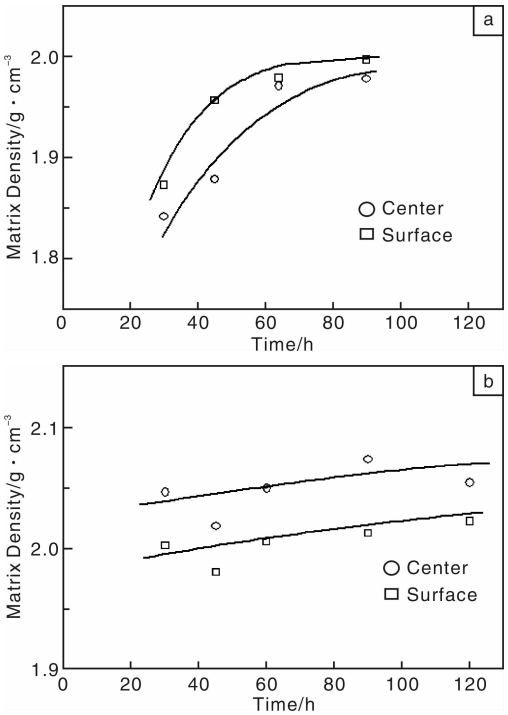

Fig. 6 Density of matrix carbon as a function of infiltration time: (a) Felt I and (b) Felt II

The extinction angle, A_e, is used for a quantitative characterization of texture. Layer thicknesses and corresponding A_e are presented in Fig. 9 (Felt I) and Fig. 10 (Felt II). The results of Fig. 9 reflect a relatively homogeneous infiltration of Felt I. The first layer is growing to a maximum thickness of 14 μm in both positions, 1A and 4B, the A_e is varying between 13° and 15°. A texture change takes place between 30 and 45 h (4B) and between 45 and 60 h (1A). Extinction angles of the second layer vary between 18° and 20° indicating an improved texture compared to the first layer.

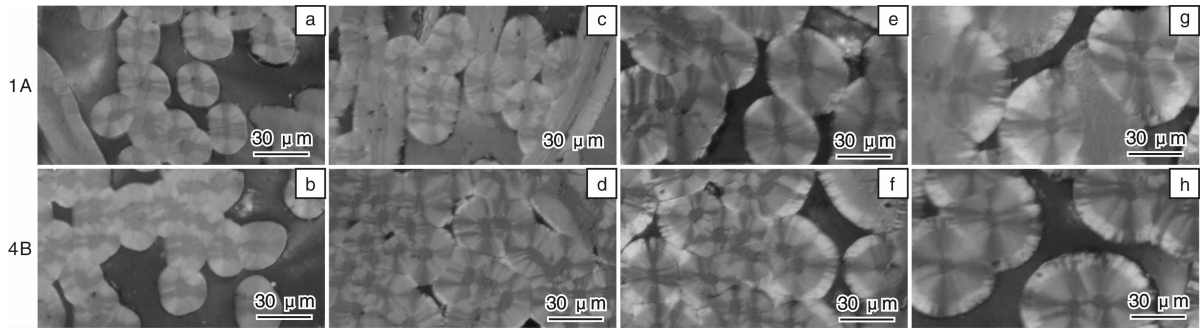

Fig. 7 Polarized-light micrographs of samples 1A (corresponds to a shortest residence time) and 4B (corresponds to a longest residence time) in Felt I infiltrated at various times showing formation and change of textures from low- to high-textured carbon: (a, b) 30 h, (c, d) 45 h, (e, f) 64 h, and (g, h) 90 h

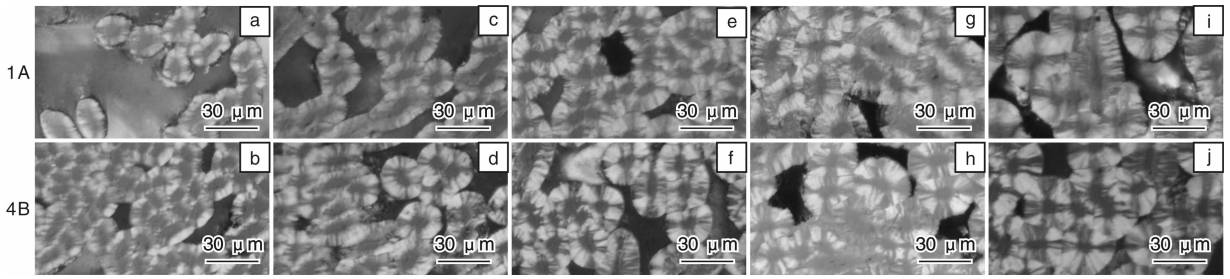

Fig. 8 Polarized-light micrographs of the sample 1A (corresponds to a shortest residence time) and 4B (corresponds to a longest residence time) in Felt II infiltrated at various times showing formation and change of textures from low-to high-textured carbon: (a, b) 30 h, (c, d) 45 h, (e, f) 60 h, (g, h) 90 h, and (i, j) 120 h

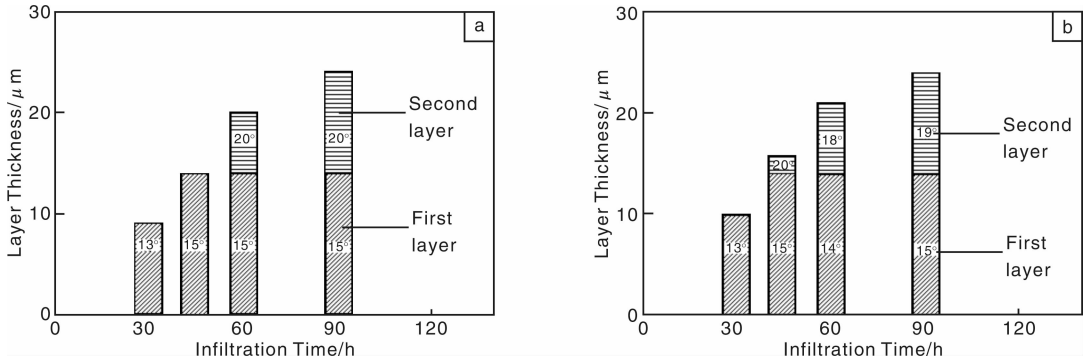

Fig. 9 Layer thickness and extinction angle, A_e, of carbon deposited in Felt I: (a) sample 1A and (b) sample 4B

Results with Felt II are different (Fig. 10). The first layer formed in the initial stage of infiltration reaches a thickness of about 2 μm, only. This value as well as an indication on its texture degree (low/medium) are derived from scanning electron micrographs presented in Fig. 11. Texture is changed already within the first 30 h, but it is noteworthy that extinction angles in position 1A reach values of about 18°, only, where as a value of about 23° was determined in position 4B. Comparing the results with both felts reveals that the influence of initial [A/V] ratio on the texture of deposited carbon is even stronger than on the kinetics of infiltration.

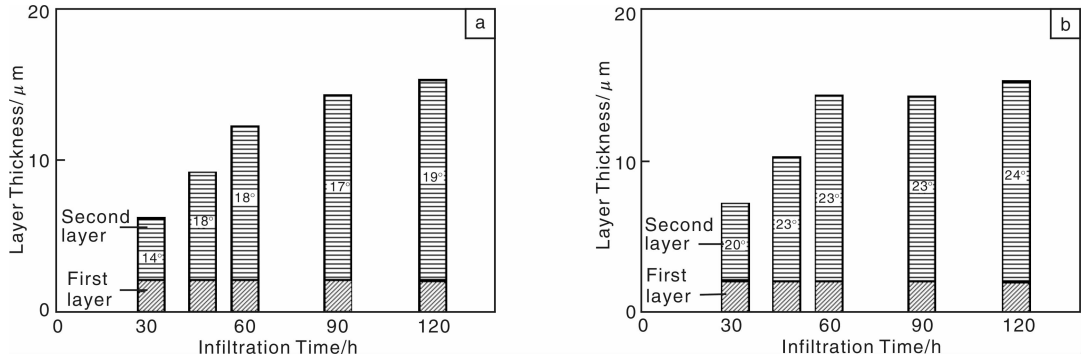

Fig. 10 Layer thickness and extinction angle, A_e, of carbon deposited in Felt II: (a) sample 1A and (b) sample 4B

4 Discussion

4.1 infiltration kinetics

Results of Fig. 2 suggest that the infiltration rates within the first 30 to 40 h are nearly constant and, even more remarkable, independent of the initial surface area or initial [A/V] ratio which differ by a factor of 2 and even 2.5, respectively. To envisualize this result the mass increase per volume, $\Delta\rho$, of both felts was calculated using Eq. (3):

$$\Delta\rho_{bulk} = \rho_{bulk} - \rho_0 \qquad (3)$$

with ρ_0 is the initial bulk density of the felt, 0.122 g/cm^3 (Felt I) and 0.244 g/cm^3 (Felt II).

Results obtained with the data of Fig. 2 are plotted in Fig. 12. They confirm constant deposition rates up to about 40h (Felt I) and about 20 – 30 h (Felt II), although the surface area and still more the [A/V] ratio of both felts have significant been increased in this stage of infiltration. This implies that correlations between surface area or [A/V] ratio and deposition rate do not exist, a conclusion which is additionally confirmed by nearly constant deposition rates in Felt I and II.

Mechanisms of carbon deposition have to be discussed for explaining the observation. Results of earlier studies indicated

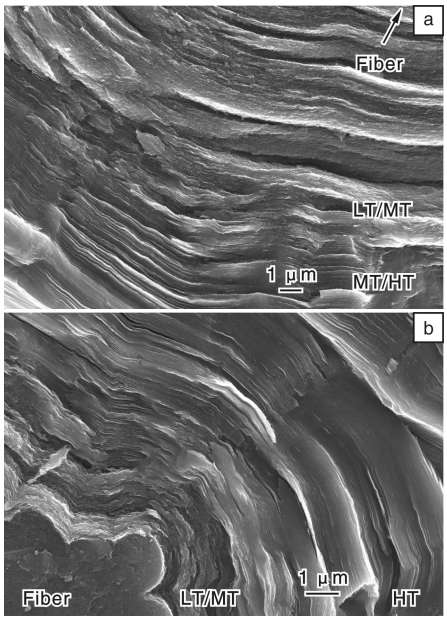

Fig. 11 Scanning electron microscopy images of a fracture surface of Felt I and Felt II after 90 h infiltration time indicating texture changes from low (LT)-, medium (MT)- to high-textured (HT) carbon

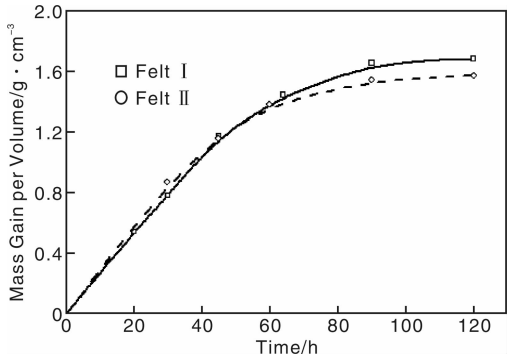

Fig. 12 Mass gain per volume of Felt I and Felt II as a function of infiltration time

that carbon may be deposited in a growth or a nucleation mechanism[23]. The growth mechanism is based on heterogeneous reactions between active sites at the growing carbon surface and reactive species from the gas phase. In this mechanism the surface area or, more precisely, the [A/V] ratio play a dominant role. The surface area correlates with the concentration of active sites, and the volume is responsible for the formation of reactive species.

In the present study, fiber preforms with a low fiber volume fraction, in other words, a low surface area and a high volume (porosity) or a low [A/V] ratio were used. Under these conditions gas phase reactions are favored, because the extent of reactive species removed from the gas phase is limited by the low surface area or low concentration of active sites. Favored gas phase reactions lead to aromatic hydrocarbon species of increasing size being able to condense on the surface. As new carbon layers are nucleated on the surface this mechanism was introduced as a nucleation mechanism. It is obvious that the surface or the [A/V] ratio do not play a role in the deposition mechanism as long as they are sufficiently small. With progressive infiltration the surface area is increasing and the free volume is decreasing simultaneously. Both processes result in a strong increase of [A/V] ratio.

It is obvious that decreasing deposition rates do not correlate with increasing surface area. An increasing [A/V] ratio causes a change of deposition chemistry: the extent of gas phase reactions is limited by the shrinking volume and surface reactions are intensified by the growing surface area. Consequences can be derived from the resulting carbon texture which reacts much stronger on a changing deposition chemistry than the deposition kinetics, as discussed later.

At a sufficiently high [A/V] ratio the mechanism of carbon deposition will change. Aromatic hydrocarbon species large enough to be condensed on the surface are not formed furthermore. Kinetics are controlled by the reaction of reactive species from the gas phase with active sites. This implies that carbon formation is based on the growth mechanism. The change from nucleation to the growth mechanism with Felt I and II will be discussed on the basis of carbon texture in the following.

An inside-outside densification was obtained with both felts as shown in Fig. 3 and 4. This phenomenon was discussed in earlier papers in great detail[18]. Concerning the present study it is noteworthy that inside-outside densification of Felt II occurred up to the final stage of densification (Fig. 4, 90 h), whereas it was apparently limited to about 64 h in the case of Felt I. Results of Fig. 5 showing the porosity of both felts after 45, 60(64) and 90 h infiltration time do not confirm this conclusion. The porosity in the "center" of Felt I is lower than that of Felt II in all stages of infiltration at and above 45 h, although the initial porosity is higher according to the lower fiber volume fraction. Additionally, it is remarkable that the porosity differences between surface and center of Felt I are higher than those of Felt II. This result suggests that inside-outside densification is even more pronounced in Felt I than in Felt II.

A possible explanation of this discrepancy between bulk density (Fig. 3, 4) and porosity data (Fig. 5) in relation to an inside-outside densification results from Fig. 6 showing the density of the matrix carbon of "center" and "surface" of both felts. Carbon densities in the "center" of Felt I are not only significantly lower than those of Felt II, but also lower than the carbon densities at the "surface", whereas Felt II exhibits higher carbon densities in the center.

The results envisualize that inside-outside densification is well defined on the basis of both, bulk density as well as porosity provided that the density of the matrix carbon is constant along the infiltration path. In the case of a density change, porosity but not the bulk density can be used to distinguish between an inside-outside or a reversed densification.

4.2 Texture of infiltrated carbon

It was already stated before that (1) deposition chemistry changes with progressive infiltration indicating a change in the deposition mechanism, and (2) texture formation reacts more sensitive or changes of deposition chemistry than kinetics. Results on texture are presented in Fig. 9 (Felt I) and Fig. 10 (Felt II).

Infiltration of Felt I (Fig. 9) is determined over broad ranges of times by formation of a medium-textured carbon ($12° < A_e < 18°$) followed by a weakly high-textured carbon ($A_e > 18°$). Differences between "surface" (sample 1A) and "center" (sample 4B) are small. The change of texture with progressive densification should result from a change of deposition, initially being dominated by nucleation and afterwards controlled by growth. Texture gradients within a layer are not resolved by PLM.

Felt II also shows a first layer with lower texture degree. This layer, however, is thin and the majority of infiltrated carbon is high-textured, especially in the "center" corresponding to an A_e of about 23°. In this case, it has also to be concluded that the texture alteration is caused by a change of the deposition mechanism. The very early alteration of texture, compared to Felt I, is a direct consequence of the higher initial [A/V] ratio.

Some earlier results may be helpful to understand above conclusions. Infiltration of Felt I at various pressures yields a pure high-textured matrix carbon at a methane pressure of 10 kPa[18], and lower texture degrees at lower as well as higher pressures. The latter result is confirmed in the present study. At very low pressures the optimum condition for formation of a high-textured carbon is not achieved; this condition is a special ratio of C2 – species and small aromatic hydrocarbon species as postulated by the particle-filler model[24,18].

The results with Felt II are similar to those obtained with a 2D fiber preform with a fiber volume fraction of 22.5%[19]. With this preform a pure high-textured carbon was obtained at a pressure of 22.5 kPa. This implies that the thin first layer of lower textured carbon formed in Felt II is excluded by the higher [A/V] ratio of that preform. Infiltration occurred exclusively under conditions of the growth mechanism at an optimum ratio between C2 – species and small aromatic hydrocarbon species.

Changes of the deposition mechanism and the texture of the resulting carbon caused by various methane pressures have perfectly been demonstrated in studies concerned with an infiltration of capillaries, 1 mm in diameter and two different lengths. In these studies it was shown that a high-textured carbon can be deposited not only under conditions of the growth mechanism, but also under conditions of the nucleation mechanism, provided that the pressure is sufficiently high. Theoretically, this could be possible with Felt I at a pressure higher than 22.5 kPa being not relevant for a CVI process.

5 Conclusions

The [A/V] ratio of a fiber preform represents a decisive parameter of CVI controlling both, kinetics of infiltration as well as texture of infiltrated carbon. An inside-outside densification of a fiber preform is possible not only under conditions of the growth mechanism, but also under conditions of the nucleation mechanism, provided that the fiber preform exhibits a sufficiently low [A/V] ratio.

This possibility, however, is less interesting from a technical point of view: (i) Methane pressures needed to produce a desired high-textured carbon will be non-realistically high. (ii) In addition, formation of such a carbon is limited with progressive densification because the increasing [A/V] ratio has the same effect like a decreasing pressure leading to medium-and low-textured carbon.

An optimum CVI process combining an inside-outside densification with the formation of a desired high-textured matrix carbon should be based on the growth mechanism of carbon deposition. Therefore, the methane pressure has to be adjusted to the [A/V] ratio of the fiber preform, preferentially in such a way, that a high-textured carbon is formed, according to the particle-filler model from an optimum ratio of small linear, mainly C2-species, and small aromatic hydrocarbon species. Low [A/V] ratios require low pressures, high ratios high pressures. A temperature of about 1100 ℃ is needed to generate the species in the gas phase.

References

[1] Hüttinger K J. CVD in Hot Wall Reactors-the Interaction between Homogeneous Gas-Phase and Heterogeneous Surface Reactions [J]. *Adv Mater*, 1998, 4(4): 151 – 58.

[2] Hüttinger K J. Fundamentals of Chemical Vapor Deposition in Hot Wall Reactors[J]. *World of Carbon*, 2003: 75 – 85.

[3] Becker A, Hüttinger K J. Chemistry and Kinetics of Chemical Vapor Deposition of Pyrocarbon-IV. Pyrocarbon Deposition from Methane in the Low Temperature Regime[J]. *Carbon*, 1998, 36 (3): 213 – 224.

[4] Brüggert M, Hu Z J, Hüttinger K J. Chemistry and Kinetics of Chemical Vapor Deposition of Pyrocarbon: VI. Influence of Temperature Using Methane as a Carbon Source[J]. *Carbon*, 1999, 37(12) : 2 021 – 2 030.

[5] Benzinger W, Hüttinger K J. Chemical Vapor Infiltration of Pyrocarbon: I. Some Kinetic Considerations[J]. *Carbon*, 1996, 34 (12): 1 465 – 1 471.

[6] Benzinger W, Hüttinger K J. Chemistry and Kinetics of Chemical Vapor Infiltration of Pyrocarbon-V. Infiltration of Carbon Fiber Felt[J]. Carbon 1999, 37(6): 941 – 946.

[7] Benzinger W, Hüttinger K J. Chemistry and Kinetics of Chemical Vapor Infiltration of Pyrocarbon-VI. Mechanical and Structural Properties of Infiltrated Carbon Fiber Felt[J]. *Carbon*, 1999, 37 (8): 1 311 – 1 322.

[8] Teubner M, Antes J, Hu Z, *et al*. The Role of the Substrate Surface Area/Reactor Volume Ratio in Chemistry and Kinetics of Chemical Vapor Deposition[J]. *J de Physique IV*, 1999, 9: 79 – 84.

[9] Antes J, Hu Z J, Zhang W G, *et al*. Chemistry and Kinetics of Chemical Vapor Deposition of Pyrocarbon: VII. Confirmation of the Influence of the Substrate Surface Area/Reactor Volume Ratio [J]. *Carbon*, 1999, 37(12): 2 031 – 2 039.

[10] Zhang W G, Hüttinger K J. Chemical Vapor Deposition of Carbon from Methane at Various Pressures, Partial Pressures and Substrate Surface Area / Reactor Volume Ratios[J]. *J Mater Sci*, 2001, 36 (14): 3 503 – 3 510.

[11] Hu Z, Hüttinger K J. Chemistry and Kinetics of Chemical Vapor Deposition of Pyrocarbon-VIII. Carbon Deposition from Methane at Low Pressures[J]. *Carbon*, 2001, 39(3): 433 – 441.

[12] Hu Z J, Hüttinger K J. Influence of the Surface Area/Volume Ratio on the Chemistry of Carbon Deposition from Methane[J]. *Carbon*, 2003, 41(8): 1 501 – 1 508.

[13] Becker A, Hu Z J, Hüttinger K J. A Hydrogen Inhibition Model of Carbon Deposition from Light Hydrocarbons [J]. *Fuel*, 2000, 79(13): 1 573 – 1 580.

[14] Zhang W G, Hüttinger K J. Chemical Vapor Infiltration of Car-

bon-Revised I: Model Simulations[J]. *Carbon*, 2001, 39(7): 1 013 – 1 022.
[15] Hu Z, Hüttinger K J. Chemical Vapor Infiltration of Carbon-Revised II: Experimental Results[J]. *Carbon*, 2001, 39(7): 1 023 – 1 032.
[16] Zhang W G, Hüttinger K J. Simulation Studies on the Chemical Vapor Infiltration of Carbon[J]. *Composites Science and Technology*, 2002, 62(15): 1 947 – 1 955.
[17] Guellali M, Oberacker R, Hoffmann M J, *et al*. Textures of Pyrolytic Carbon Formed in the Chemical Vapor Infiltration of Capillaries[J]. *Carbon*, 2003, 41(1): 97 – 104.
[18] Zhang W G, Hüttinger K J. Chemical Vapor Infiltration of Carbon Fiber Felt: Optimization of Densification and Carbon Microstructure[J]. *Carbon*, 2002, 40(14): 2 529 – 1 545.
[19] Zhang W G, Hüttinger K J. Chemical Vapor Infiltration of 2D Carbon Fiber Preform: Kinetics of Densification and Carbon Microstructure[J]. *Carbon*, 2003, 41(12): 2 325 – 2 337.
[20] Zhang W G, Hüttinger K J. Texture Formation of Pyrolytic Carbon in Chemical Vapor Deposition and Infiltration[J]. *New Carbon Materials*, 2006.
[21] Hu Z, Zhang W G, Hüttinger K J. An Extended Interpretation of Chemical Vapor Infiltration of Carbon[J]. *J de Physique IV*, 2001: 307 – 313.
[22] Reznik B, Gerthsen D, Zhang W G, *et al*. Texture Changes in the Matrix of an Infiltrated Carbon Fiber Felt Studied by Polarized Light Microscopy and Selected Area Electron Diffraction [J]. *Carbon*, 2003, 41(2): 376 – 380.
[23] Hu Z, Hüttinger K J. Mechanisms of Carbon Deposition-a Kinetic Approach[J]. *Carbon*, 2002, 40(4): 624 – 628.
[24] Dong G L, Hüttinger K J. Consideration of Reaction Mechanisms Leading to Pyrolytic Carbon of Different textures[J]. *Carbon*, 2002, 40(14): 2 515 – 2 528.
[25] Reznik B, Gerthson D, Hüttinger K J. Micro-and Nanostructure of Carbon Matrix of Infiltrated Carbon Fiber Felt[J]. *Carbon*, 2001, 39(2): 215 – 229.
[26] Reznik B, Hüttinger K J. On the Terminology for Pyrolytic Carbon[J]. *Carbon*, 2002, 40(4): 621 – 624.
[27] Bourrat X, Trouvat B, Limousin G, *et al*. Pyrocarbon Anisotropy as Measured by Electron Diffraction and Polarized Light[J]. *J Mater Res*, 2000, 15(1): 92 – 101.
[28] Bortchagovsky E G, Reznik B, Gerthsen D, *et al*. Optical Properties of Pyrolytic Carbon Deposits Deduced from Measurements of Extinction Angle by Polarized Light Microscopy[J]. *Carbon*, 2003, 41: 2 427 – 2 451.
[29] Vallerot J M, Bourrat X. Pyrocarbon Optical Properties in Reflected Light[J]. *Carbon*, 2006, 44: 1 565 – 1 571.
[30] Drescher M, Hüttinger K J, Dormann E. Pyrolytic Carbon Layers-an Electron Spin Resonance Analysis[J]. *Carbon*, 2003, 41: 773 – 783.
[31] Pfrang A, Hüttinger K J, Schimmel Th. Adhesion Imaging of Carbon Fiber Reinforced Materials in the Pulsed Force Mode of the AFM[J]. *Surface Interface Anaysis*, 2002, 33: 96 – 100.
[32] Chen T F, Reznik B, Gerthsen D, *et al*. Microscopical Study of Carbon/Carbon Composites Obtained by Chemical Vapor Infiltration of 0°/0° /90°/90° Carbon Diber Preforms[J]. *Carbon*, 2005, 43 (15): 3 088 – 3 098.
[33] Hu Z J, Zhang W G, Hüttinger K J, *et al*. Influence of Pressure, Temperature and Surface Area/Volume Ratio on the Texture of Pyrolytic Carbon Deposited from Methane[J]. *Carbon*, 2003, 41(4): 749 – 758.

日本首次合成出间隙型铝合金氢化物 有望为燃料电池储氢

据物理学家组织网2013年11月5日报道，日本科学家发现铝可用来为燃料电池存储氢气。铝是地壳中含量最丰富的金属元素，广泛应用于航空、建筑和汽车等领域。

最近，日本原子能研究机构和日本东北大学组成的联合科研团队宣布，他们使用以铝(Al)为主要原料的合金，在全球首次成功合成出间隙型铝合金氢化物。这项研究成果有望为燃料电池汽车提供更轻便的储氢合金。研究成里发表在美国物理联合会(API)出版的《应用物理快报·材料学》杂志上。

燃料电池车要求储氢合金轻量化。此前的储氢合金除了镁(Mg)等外，大多数使用镍(Ni)、钯(Pd)等比较重的金属，而以铝为原料制造的合金氢化物更加实用，因为铝轻质且耐腐蚀。

以铝为主要原料的氢化物方面，虽然科学家们已经制造出了络合铝氢化物，但一直没有出现兼具储氢和放氢两大功能的材料。另一方面，间隙型氢化物内的氢原子占据了金属原子之间的空隙，因此被科学家们认为是燃料电池汽车安全且高效的储氢手段。尽管已经有人用镁、钠和硼制造出了间隙型氢化物，但并不实用。迄今为止，还没有人以铝为主要原料，制造出间隙型铝合金氢化物。

研究人员让铝与铜的合金 Al_2Cu 在高温(800多摄氏度)高压(10万个大气压)环境下与氢气发生反应，合成了氢化物 Al_2CuH。随后，科学家们使用世界上能量最高的第三代同步辐射光源——日本大型同步辐射设施 SPring－8 对合成环境及对氢化物的晶体结构和电子结构进行了检查和分析，确认能够合成出以铝为主要原料的间隙型铝合金氢化物。

科学家们表示："尽管合成需要的环境非常苛刻，氢的浓度也比较低，合成出来的物质也不一定能直接使用，但最新实验证实，我们的确能合成出以铝为原料的间隙型铝合金氢化物。我们计划在更加温和的环境下合成出同样的材料，这样获得的产品能有效地为燃料电池汽车存储氢气。"

(来源：中国科技网)